Spin dynamics in the manganese tetramer compound α-$MnMoO_4$

2009 J. Phys.: Condens. Matter 21 026019

(http://iopscience.iop.org/0953-8984/21/2/026019)

J. Phys.: Condens. Matter **21** (2009) 026019 (7pp) doi:10.1088/0953-8984/21/2/026019

Spin dynamics in the manganese tetramer compound α-$MnMoO_4$

P S Häfliger[1], S T Ochsenbein[2], B Trusch[2], H-U Güdel[2] and A Furrer[1]

[1] Laboratory for Neutron Scattering, ETH Zurich and PSI Villigen, CH-5232 Villigen PSI, Switzerland
[2] Department of Chemistry and Biochemistry, University of Bern, CH-3012 Bern, Switzerland

E-mail: albert.furrer@psi.ch

Received 31 October 2008
Published 11 December 2008
Online at stacks.iop.org/JPhysCM/21/026019

Abstract

α-$MnMoO_4$ is a tetrameric magnetic cluster system which undergoes a transition to three-dimensional antiferromagnetic order at $T_N = 10.7$ K. In the ordered state the Mn^{2+} spins ($s_v = 5/2$) are ferromagnetically aligned within the tetramer, resulting in a total cluster spin $S = 10$. The magnetic excitation spectrum consists of eight excitation modes of tetramer origin propagating in the whole reciprocal space. From single-crystal inelastic neutron scattering investigations the three-dimensional coupling scheme is rationalized in the framework of a tetramer-based dispersion model. The tetramer states and the energy dispersion of all the magnetic excitations are described by Heisenberg-like intra- and intercluster exchange interactions, respectively, thus α-$MnMoO_4$ is a suitable tetrameric model system to study the interplay of these interactions.

1. Introduction

The interplay of strong and weak exchange interactions in insulating magnetic materials can lead to very interesting phenomena such as low-dimensional magnets and single-molecule magnets (SMMs). The latter are of considerable current interest, both from a fundamental point of view and for their application potential as the smallest nanomagnetic units capable of storing a bit of information [1]. SMMs represent the extreme situation, in which intermolecular interactions are negligibly small, thus giving rise to the typical SMM phenomena of slow magnetic relaxation of single molecules at low temperatures as well as the steps in the hysteresis curves resulting from molecular level crossings. New phenomena emerge when exchange or dipole–dipole interactions between the molecular clusters are no longer negligible. A well documented system is the compound $[Mn_4O_3Cl_4(O_2CEt)_3(py)_3]_2{\cdot}8MeCN$, in which the tetrameric Mn^{3+}/Mn^{4+} clusters occur as hydrogen-bridged dimers in the crystal. As a result, the exchange-induced level ordering changes significantly, and it is well accounted for by a theoretical dimer model [2]. A similar model was employed to interpret the magnetic properties of the cluster compound $[Mn_4O_3(OSiMe_3)(OAc)_3(dbm)_3]$ [3]. But in this case, the clusters do not occur as dimers, and the intercluster interactions extend throughout the crystal in all directions. The dimer model was used for simplicity, because the magnetic data did not contain enough information to allow a physically more realistic treatment of the intermolecular interactions.

The title compound α-$MnMoO_4$ contains tetrameric oxo-bridged manganese clusters, in which the Mn^{2+} ions occupy the corners of a rhomb, as shown in figure 1(a). These are linked by non-magnetic $(MoO_4)^{2-}$ groups in the three-dimensional structure. In contrast to molecular cluster materials, this will lead to significant intercluster interactions. We thus have a model system to study the interplay of intracluster and intercluster interactions. And since we have a single crystal, we obtain a very detailed experimental picture of this interplay, which allows a physically realistic model treatment. Another unique feature of the title compound is the ferromagnetic coupling of the Mn^{2+} spins within the tetramers, *vide supra*, which leads to a very large cluster spin ground state $S = 10$.

The inelastic neutron scattering (INS) technique has proven to be a highly potent tool to determine the exchange interactions in magnetic cluster systems. While there is a large body of information on intracluster interactions in both molecular magnetic compounds [4] and insulators doped with

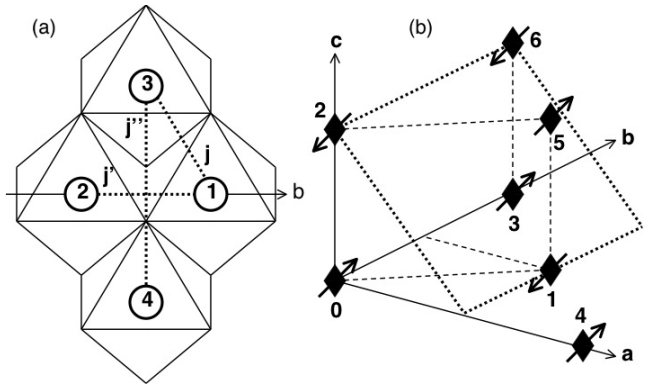

Figure 1. (a) The Mn_4O_{16} cluster in α-$MnMoO_4$ consisting of four edge-sharing MnO_6 octahedra with the Mn^{2+} ions shown as circles and the oxygen ions at the corners. The Mn(1)–Mn(2) bond is along the b-axis. The dotted lines mark the intracluster exchange parameters j, j', and j''. (b) Antiferromagnetic arrangement of the Mn $_4$ clusters (marked by diamonds) in α-$MnMoO_4$ up to the sixth coordinating shell. The arrows denote the spin orientation, which is close to the [1, 0, 1] direction. The dotted lines mark the sublattice plane defined by $2x + z - 1 = 0$.

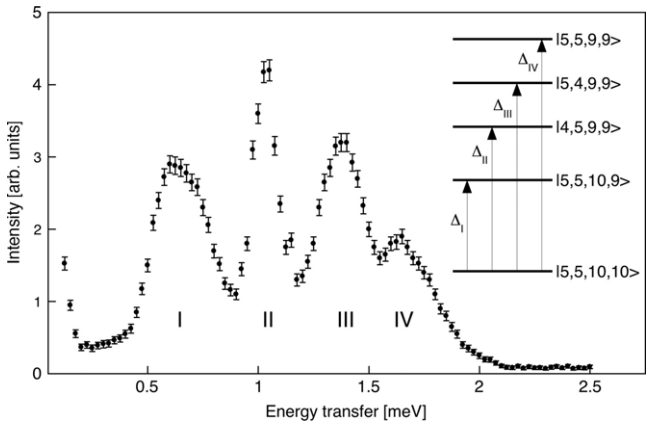

Figure 2. Energy spectrum of neutrons scattered from polycrystalline α-$MnMoO_4$ at 1.5 K [8]. The inset shows the resulting energy level sequence in $|S_{12}, S_{34}, S, M\rangle$ tetramer notation.

magnetic ions [5], INS experiments to unravel intercluster interactions are rather scarce and moreover only available for dimer systems [6, 7]. To our knowledge the present work performed for the compound α-$MnMoO_4$ is the first to address the issue of intercluster interactions in a magnetic tetramer system. Preliminary INS experiments have been performed on a polycrystalline sample of α-$MnMoO_4$ [8], which provided information on the intra-tetramer interactions. However, in order to obtain information on the inter-tetramer interactions, INS experiments on a single crystal are indispensable.

Monoclinic α-$MnMoO_4$ ($a = 10.469$ Å, $b = 9.516$ Å, $c = 7.143$ Å, $\beta = 106.3°$ [9]) contains Mn_4O_{16} clusters of four edge-sharing MnO_6 octahedra as shown schematically in figure 1(a). These clusters have C_{2h} symmetry and give rise to intracluster superexchange between the rhombically arranged Mn^{2+} spins through the shared edges. The clusters are linked by molybdate tetrahedra to form an extended magnetic network. Long-range antiferromagnetic order exists below $T_N = 10.7$ K with almost saturated Mn^{2+} moments at low temperatures [10]. The order is characterized by a ferromagnetic alignment of the Mn^{2+} spins ($s_\nu = 5/2$) within the cluster, resulting in a total cluster spin $S = 10$. The antiferromagnetic coupling between the clusters is defined by the magnetic ordering wavevector $\mathbf{q}_0 = (1, 0, 1/2)$. The magnetic unit cell is obtained by doubling the c-axis of the chemical unit cell, i.e., there are eight Mn^{2+} ions (or two Mn tetramers) in the magnetic unit cell, and therefore the magnetic excitation spectrum is composed of eight individual branches.

The present work is organized as follows. Section 2 provides a short summary of the experimental details. The theoretical background is described in section 3. The main part of the paper is section 4, which presents the experimental data as well as their analysis in terms of the excitation model outlined in the preceding section. Finally, the results are discussed and some conclusions are given in section 5.

2. Experiment

The ingredients for the sample synthesis were 33.0 g (0.47 mol) MnO and 67.0 g (0.47 mol) MoO_3, which were ground together and placed in a platinum crucible. The mixture was heated to 1200 °C for 10 h, and then cooled down to room temperature at a rate of 300 °C h^{-1}. The solidified melt was used as starting material for the crystal growth by the Czochralski method. The platinum crucible was inductively heated to 1200 °C, and a platinum wire was put into the melt. Slowly retracting the wire from the melt over a temperature gradient, while rotating it, led to a cylindrical product attached to the wire. X-ray diffraction revealed that the final product was a 10 g single crystal of α-$MnMoO_4$.

The INS experiments were carried out on the triple-axis spectrometers RITA and TASP at the spallation neutron source SINQ at PSI Villigen. The instruments were operated at fixed final energies of 4.9, 3.8, and 2.5 meV, giving energy resolutions at the elastic line of 238, 141, and 66 μeV, respectively. A cooled beryllium filter was placed in front of the analyser in order to prevent higher-order reflections. The single crystal was mounted in a He cryostat to keep the temperature at 1.5 K for all experiments. The orientation of the single crystal was varied in order to have the reciprocal (H, K, 0), (H, 0, L), or (0, K, L) plane parallel to the scattering plane.

3. Theoretical background

Preliminary INS experiments were performed for polycrystalline α-$MnMoO_4$ as shown in figure 2 [8]. At $T = 1.5$ K four well defined transitions with varying widths and labelled from I to IV were observed. The results could be rationalized on the basis of the Oguchi model, in which the dominant intracluster interactions are treated exactly, whereas the interactions with the remainder of the system are approximated by an effective molecular field [11]. Thus, the spin Hamiltonian of a Mn tetramer is

$$\mathcal{H} = \mathcal{H}_{\text{intra}} + \mathcal{H}_{\text{mf}}. \qquad (1a)$$

In the Heisenberg model, the intracluster Hamiltonian is defined by

$$\mathcal{H}_{\text{intra}} = -2j(\mathbf{s}_1\cdot\mathbf{s}_3+\mathbf{s}_1\cdot\mathbf{s}_4+\mathbf{s}_2\cdot\mathbf{s}_3+\mathbf{s}_2\cdot\mathbf{s}_4)-2j'\mathbf{s}_1\cdot\mathbf{s}_2-2j''\mathbf{s}_3\cdot\mathbf{s}_4, \tag{1b}$$

where j, j', and j'' denote the exchange parameters as indicated in figure 1(a), and $s_\nu = 5/2$ is the spin quantum number of an individual Mn^{2+} ion. For a complete characterization of the tetramer states, we need additional spin quantum numbers resulting from the vector sums $\mathbf{S}_{12} = \mathbf{s}_1+\mathbf{s}_2$, $\mathbf{S}_{34} = \mathbf{s}_3 + \mathbf{s}_4$, and $\mathbf{S} = \mathbf{S}_{12} + \mathbf{S}_{34}$ with $0 \leqslant S_{12} \leqslant 5$, $0 \leqslant S_{34} \leqslant 5$, and $|S_{12} - S_{34}| \leqslant S \leqslant (S_{12} + S_{34})$, respectively. The molecular-field Hamiltonian at the tetramer site is then given by

$$\mathcal{H}_{\text{mf}} = -g\mu_{\text{B}}H_{\text{mf}}\sum_{\nu=1}^{4}s_\nu^z = -g\mu_{\text{B}}H_{\text{mf}}S^z \tag{1c}$$

where g is the spectroscopic splitting factor, μ_{B} the Bohr magneton, and H_{mf} the molecular field resulting from the interaction with all Mn^{2+} ions which do not belong to the tetramer. The eigenvalues of the Hamiltonian (equations (1)) can easily be shown to be

$$\begin{aligned}E(S_{12}, S_{34}, S, M) = &-j[S(S+1) - S_{12}(S_{12}+1)\\ &- S_{34}(S_{34}+1)] - j'[S_{12}(S_{12}+1) - 2s_i(s_i+1)]\\ &- j''[S_{34}(S_{34}+1) - 2s_i(s_i+1)] - g\mu_{\text{B}}H_{\text{mf}}M,\end{aligned} \tag{2}$$

where $-S \leqslant M \leqslant S$. The energy level sequence of the states $|S_{12}, S_{34}, S, M\rangle$ associated with transitions I–IV is shown as an inset in figure 2. The energies Δ_r of the transitions out of the ground state $|5, 5, 10, 10\rangle$ are given by

$$\begin{aligned}\Delta_{\text{I}} &= g\mu_{\text{B}}H_{\text{mf}}, \qquad \Delta_{\text{II}} = 10j + 10j' + g\mu_{\text{B}}H_{\text{mf}},\\ \Delta_{\text{III}} &= 10j + 10j'' + g\mu_{\text{B}}H_{\text{mf}}, \qquad \Delta_{\text{IV}} = 20j + g\mu_{\text{B}}H_{\text{mf}}.\end{aligned} \tag{3}$$

In [8] the identification of the tetramer states with the transitions I–IV was based on considerations of the sign and the size of the exchange parameters, but could not really be proven by the experimental data. We will show in the present work that INS experiments on a single crystal give enough information to unambiguously determine the symmetry of the different excitation levels.

The widths of the inelastic lines I–IV in figure 2 reflect the dispersive behaviour of the transitions due to the intercluster interactions, which are described in the Heisenberg model by the Hamiltonian

$$\mathcal{H}_{\text{inter}} = -2\sum_{(nm,\nu\mu)} j_{nm,\nu\mu}\mathbf{s}_{n\nu}\cdot\mathbf{s}_{m\mu}. \tag{4}$$

Equation (4) considers interactions between neighbouring tetramers $\langle nm\rangle$, mediated by all the spins $\nu = \{1, 2, 3, 4\}$ and $\mu = \{1, 2, 3, 4\}$ at sites n and m, respectively. However, equation (4) gives rise to a very large number of exchange parameters $j_{nm,\nu\mu}$ which cannot be determined reliably from the dispersion relations for a complicated system like α-$MnMoO_4$. More specifically, the coupling of two tetrameric units involves $4 \times 4 = 16$ individual exchange parameters, and this number is likely to be tripled by considering the dispersion spectra in three dimensions. Therefore we adopt a model which was successfully used for the quantum spin dimer compounds $KCuCl_3$ [7] and $TlCuCl_3$ [12]. It describes the intercluster interactions by the Heisenberg Hamiltonian

$$\mathcal{H}_{\text{inter}} = -2\sum_{n,m} J_{nm}\mathbf{S}_n\cdot\mathbf{S}_m, \tag{5}$$

where the $\mathbf{S}_n$ and $\mathbf{S}_m$ are spin operators of the tetramers at sites n and m, respectively, and J_{nm} is the effective exchange coupling between them. Figure 1(b) shows the arrangement of the six nearest-neighbour tetramers, which were considered in the sum of equation (5) in the present work.

We now model the dispersive behaviour of the excitations on the basis of the intracluster and intercluster Hamiltonians (1*b*) and (5), respectively. The intracluster interaction provides the energy scales corresponding to the transition energies Δ_r defined by equation (3), and the intercluster interactions are considered perturbatively to yield the dispersion relations through the Fourier transform of the couplings J_{nm} between the tetramers [7, 12]:

$$\hbar\omega(\mathbf{q})_r = \Delta_r - [J(\mathbf{q}) \pm |J'(\mathbf{q})|]. \tag{6}$$

Since, according to the antiferromagnetic structure of α-$MnMoO_4$, the tetramers are located on two sublattices with opposite staggered magnetization, we have to distinguish the Fourier transforms of the intra- and inter-sublattice exchange parameters J_{nm} by $J(\mathbf{q})$ and $J'(\mathbf{q})$, respectively, giving rise to a splitting into acoustic and optic branches indicated in equation (6) by the + and − sign, respectively. $J(\mathbf{q})$ is always real, while $J'(\mathbf{q})$ is complex if the vector joining sites on different tetramer sublattices is not a lattice vector. The dispersion relation (6) is valid in the limit $|J(\mathbf{q}) \pm |J'(\mathbf{q})|| \ll \Delta_r$, thus it can be rewritten as

$$\hbar\omega(\mathbf{q})_r = \sqrt{\Delta_r^2 - 2\Delta_r[J(q) \pm |J'(q)|]}, \tag{7}$$

which is an RPA-like expression reminding us of the random-phase approximation [13].

The neutron cross-section for magnetic scattering by the transition $|S_{12}, S_{34}, S, M\rangle \rightarrow |S'_{12}, S'_{34}, S', M'\rangle$ is given by [13]

$$\frac{\mathrm{d}^2\sigma}{\mathrm{d}\Omega\,\mathrm{d}\omega} \propto F^2(\mathbf{Q})U(\mathbf{Q})[1 \pm \cos(\varphi)]\sum_\alpha\left[1 - \left(\frac{Q_\alpha}{Q}\right)^2\right]. \tag{8a}$$

$F(\mathbf{Q})$ is the magnetic form factor, and $U(\mathbf{Q})$ corresponds to the structure factor $S(\mathbf{Q}) = \sum_{\nu\mu}\exp\{\mathrm{i}\mathbf{Q}\cdot(\mathbf{R}_\nu - \mathbf{R}_\mu)\}$ of the tetramer, weighted by the transition matrix elements A_ν according to

$$U(\mathbf{Q}) = \sum_{\nu,\mu=1}^{4}\exp\{\mathrm{i}\mathbf{Q}\cdot(\mathbf{R}_\nu - \mathbf{R}_\mu)\}A_\nu A_\mu, \tag{8b}$$

where $\mathbf{Q}$ is the scattering vector, $\mathbf{R}_\nu$ the position of the Mn^{2+} ions in the tetramer, and the + and − signs refer to the acoustic and optic branches, respectively. Since all the transitions I–IV

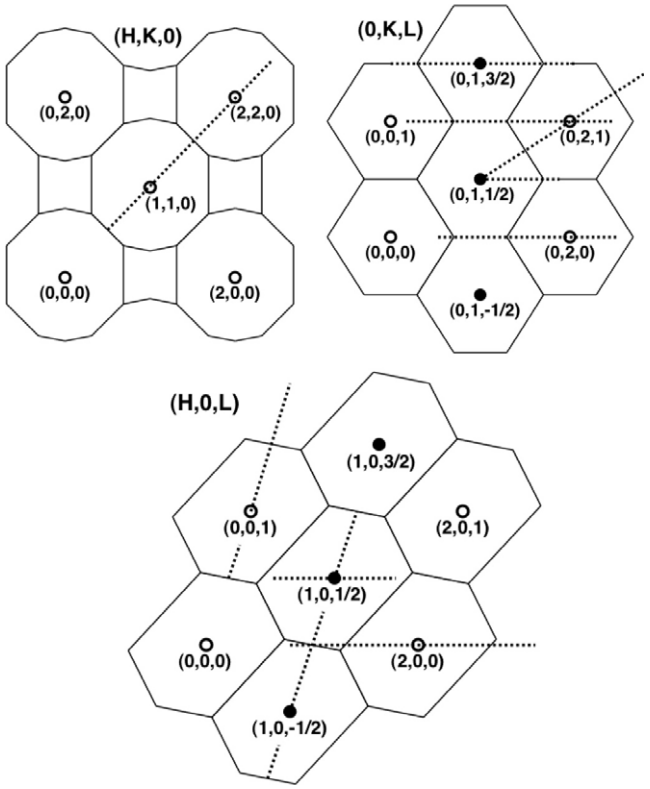

Figure 3. Projections of the Brillouin zones onto the reciprocal $(H, K, 0)$, $(H, 0, L)$, and $(0, K, L)$ planes. Open and full circles denote nuclear and magnetic Bragg peaks, and the corresponding Brillouin zones are called optic and acoustic zones, respectively. The dashed lines show the scans performed in the present experiments.

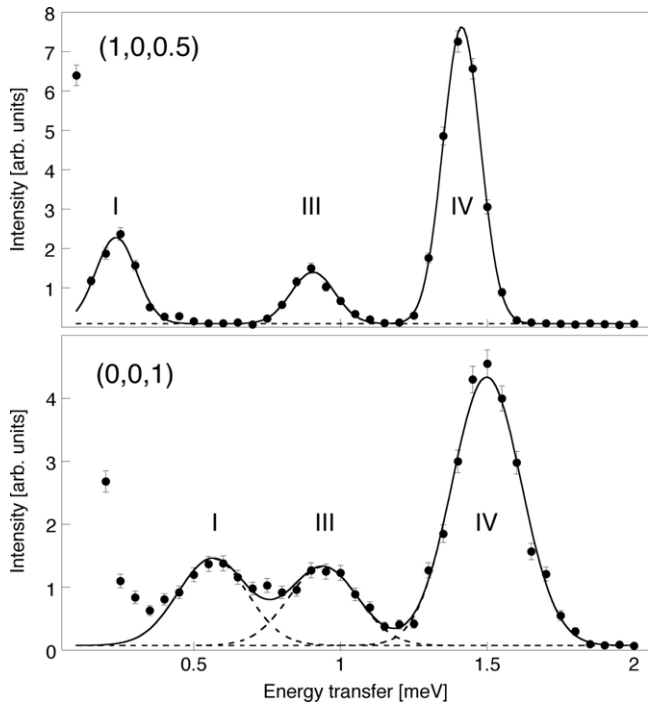

Figure 4. Energy spectra of neutrons scattered from α-$MnMoO_4$ in the centre of the acoustic and the optic Brillouin zones at (1, 0, 0.5) and (0, 0, 1), respectively. The lines are Gaussian fits to the data.

are governed by the selection rule $\Delta M = -1$, the product $A_\nu A_\mu$ is given by [8]

$$A_\nu A_\mu = \langle S_{12}, S_{34}, S, M|s_\nu^+|S'_{12}, S'_{34}, S', M'\rangle \times\langle S'_{12}, S'_{34}, S', M'|s_\mu^-|S_{12}, S_{34}, S, M\rangle. \quad (8c)$$

The phase φ in equation (8*a*) is defined through

$$J'(\mathbf{Q}) = J'(\mathbf{q})\exp\{-\mathrm{i}\boldsymbol{\tau}\cdot\boldsymbol{\rho}\} = |J'(\mathbf{q})|\exp\{-\mathrm{i}\varphi\}, \quad (9)$$

with $\boldsymbol{\tau}$ being a reciprocal lattice vector and $\boldsymbol{\rho}$ the vector connecting the two tetramer sublattices. Some vanishing matrix elements A_ν may extinguish some of the 16 terms of the function $U(\mathbf{Q})$, giving zero weight to the corresponding terms of the structure factor $S(\mathbf{Q})$. In particular, the structure factors associated with transitions II and III are reduced to the form

$$\begin{aligned}&\text{Transition II: } S(\mathbf{Q}) = 1 - \cos[\mathbf{Q}\cdot(\mathbf{R}_1 - \mathbf{R}_2)],\\ &\text{Transition III: } S(\mathbf{Q}) = 1 - \cos[\mathbf{Q}\cdot(\mathbf{R}_3 - \mathbf{R}_4)].\end{aligned} \quad (10)$$

As shown in figure 1(a), the vector $\mathbf{R}_1 - \mathbf{R}_2$ is parallel to the b-axis, thus transition II vanishes for $\mathbf{Q} = (x, 0, 0)$ and $\mathbf{Q} = (0, 0, x)$. Similarly, the vector $\mathbf{R}_3 - \mathbf{R}_4$ is perpendicular to the b-axis, thus transition III cannot be observed for $\mathbf{Q} = (0, x, 0)$.

4. Results and data analysis

Most of the INS experiments were carried out with the scattering vector $\mathbf{Q}$ in the reciprocal $(H, 0, L)$ and $(0, K, L)$ planes as shown in figure 3. These planes are characterized by a network of acoustic and optic Brillouin zones, so that both the acoustic and the optic excitation branches can be observed. The acoustic and optic Brillouin zones are associated with the magnetic and nuclear Bragg peaks, respectively. A few measurements were also performed in the reciprocal $(H, K, 0)$ plane, which, however, contains only optic Brillouin zones. All these experiments confirmed the preliminary assignment of the transitions suggested from the powder data [8]; in particular, we could confirm the absence of transition II for scans along $\mathbf{Q} = (x, 0, 0)$ and $\mathbf{Q} = (0, 0, x)$ as well as the absence of transition III for scans along $\mathbf{Q} = (0, x, 0)$.

In order to demonstrate the power of INS experiments on single crystals, we show in figure 4 the results obtained for $q = 0$ excitations in the centre of both the acoustic and the optic Brillouin zones (1, 0, 0.5) and (0, 0, 1), respectively. The peaks can readily be assigned to transitions I, III, and IV, since transition II is absent at $\mathbf{Q} = (0, 0, 1)$ due to the vanishing structure factor. We recognize that the energies of the acoustic excitations are lower than those of the optic excitations for all transitions, but the most pronounced energy shift occurs for transition I. The results of all the INS measurements are presented in figures 5–7 for some major symmetry directions. Data taken for different scattering vectors $\mathbf{Q}$ were reduced to excitation wavevectors $\mathbf{q}$ according to $\mathbf{Q} = \boldsymbol{\tau} + \mathbf{q}$. The overall dispersion of the magnetic excitations is of the order of 0.3 meV, in agreement with the observed peak broadening of

Table 1. Model parameters J_n and Δ_r defined by equations (5) and (6) determined for α-$MnMoO_4$. **d** is the vector joining the interacting tetramers; d denotes the modulus of **d**. A, fit to all transitions I–IV; B, fit to transition I; C, fit to transitions II–IV. χ^2 denotes the standard deviation of the calculated energies from those measured.

			J_n (μeV), Δ_r		
J_n, Δ_r	**d**	d (Å)	Fit A	Fit B	Fit C
J_1 ↑↓	±(1/2, 1/2, 0) ±(−1/2, 1/2, 0)	7.08	−6(3)	−15(2)	−5(2)
J_2 ↑↓	±(0, 0, 1)	7.14	−2(3)	−9(1)	1(3)
J_3 ↑↑	±(0, 1, 0)	9.52	16(3)	18(2)	16(3)
J_4 ↑↑	±(1, 0, 0)	10.47	50(8)	47(3)	53(7)
J_5 ↑↑	±(1/2, 1/2, 1) ±(−1/2, 1/2, 1) ±(1/2, −1/2, 1) ±(−1/2, −1/2, 1)	11.07	13(4)	3(1)	16(3)
J_6 ↑↓	±(0, 1, 1) ±(0, −1, 1)	11.90	−5(4)	−8(1)	−2(3)
Δ_I (meV)			0.61(2)	0.64(2)	—
Δ_{II} (meV)			1.12(2)	—	1.12(2)
Δ_{III} (meV)			1.34(3)	—	1.34(3)
Δ_{IV} (meV)			1.71(3)	—	1.72(3)
χ^2			4.0	1.0	3.8

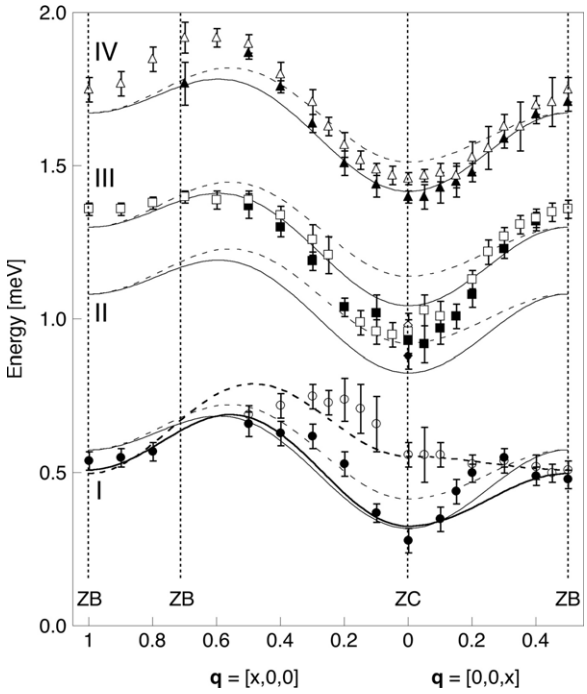

Figure 5. Dispersion of the four excitation branches I–IV observed for α-$MnMoO_4$ for the [x, 0, 0] and [0, 0, x] directions at 1.5 K. The circles, diamonds, squares, and triangles refer to the excitation branches I, II, III, and IV, respectively. The full and open symbols denote the acoustic and optic excitations, respectively. The full and dashed lines correspond to the calculated dispersion of the acoustic and optic branches, respectively, using the parameters of fit A. The bold lines refer to the calculated dispersion of the excitation branch I using the parameters of fit B. The dotted lines labelled by ZC and ZB mark the zone centre and the zone boundary, respectively.

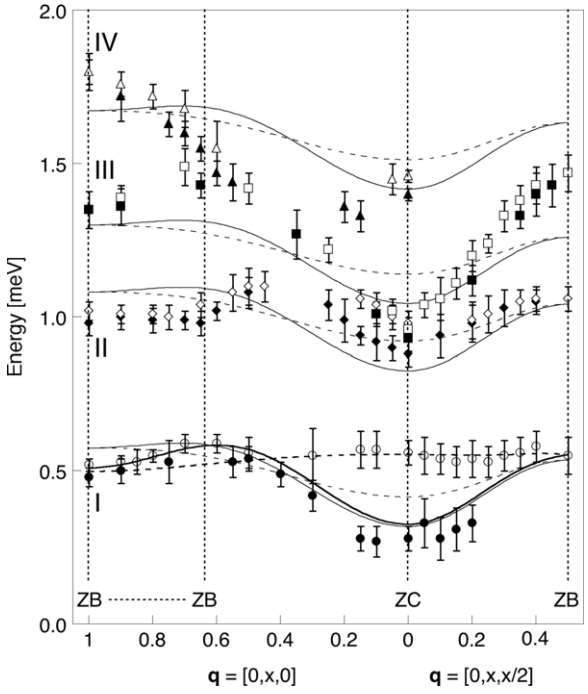

Figure 6. Dispersion of the four excitation branches observed for α-$MnMoO_4$ for the [0, x, 0] and [0, x, $x/2$] directions at 1.5 K. The symbols and lines are as in figure 5.

the powder data displayed in figure 2. The dispersion of the acoustic branch of the lowest excitation I shows the expected softening near the magnetic Bragg points, where the Fourier transformed exchange function $J(\mathbf{q}) + |J'(\mathbf{q})|$ has its absolute maximum.

We now proceed to analyse the observed excitations according to equation (6). A least-squares fitting procedure was applied to the observed dispersion curves for which we considered exchange couplings J_n up to the sixth coordinating shell as listed in table 1 (by placing the tetramer at site m at the origin, we can skip the index m of J_{nm} in equation (5); see figure 1(b)). In a first step we performed a simultaneous

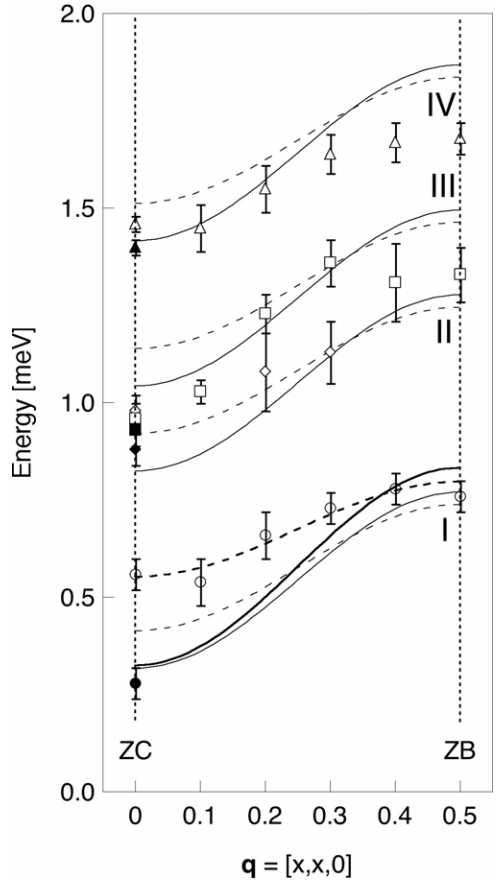

Figure 7. Dispersion of the four excitation branches observed for α-$MnMoO_4$ for the $[x, x, 0]$ direction at 1.5 K. The symbols and lines are as in figure 5.

fitting of all the excitation branches I–IV (fit A). The second fit was restricted to the lowest-lying excitation branch I alone (fit B). Finally, a simultaneous fitting of the excitation branches II–IV was carried out (fit C). The choice of these different fits is motivated by the different nature of the four transitions, $\Delta S = 0$ for transition I and $\Delta S = -1$ for transitions II–IV (see the inset of figure 2). The calculated dispersion curves for fits A and B are shown in figure 5–7 (the results of fit C are only marginally different from A). The acoustic and optic branches turn out to be almost degenerate at the zone boundary, but these are accidental degeneracies, and only at $\mathbf{q} = (0, 1/2, 1/4)$ is the degeneracy dictated by symmetry.

5. Discussion and conclusions

The model parameters Δ_r listed in table 1 are distinctly different from the mean transition energies observed in the powder experiments [8] (see figure 2), which demonstrates the importance of single-crystal experiments for a precise determination of the intracluster interactions. With the help of equation (3) we determine the intracluster exchange parameters and the molecular field to be

$$j = 54(3)\ \mu\text{eV}, \qquad j' = -4(7)\ \mu\text{eV},$$

$$j'' = 18(8)\ \mu\text{eV}, \qquad H_{\text{mf}} = 5.4(3)\ \text{T}.$$

Some of these values considerably differ from the parameters $j = 51\ \mu$eV, $j' = -19\ \mu$eV, $j'' = 0$, $H_{\text{mf}} = 6.3$ T derived from the powder experiments [8].

The net coupling within the tetramers in α-$MnMoO_4$ is ferromagnetic, which is very unusual for Mn^{2+} based magnets. Since each Mn^{2+} ion has five unpaired electrons, the net exchange between two Mn^{2+} ions is actually the sum of $5 \times 5 = 25$ orbital contributions. We conclude that the specific geometries of the Mn–O–Mn bridges in α-$MnMoO_4$ lead to an almost complete cancellation of the 25 contributions, with the resulting j values being much smaller than the individual orbital contributions.

The dispersion model based on equation (6) turned out to be a reasonable approximation for the interpretation of the magnetic excitations in α-$MnMoO_4$. With the overall dispersion of about 0.3 meV being defined by the Fourier transformed exchange function, the condition for the applicability of equation (6), $|J(\mathbf{q}) \pm |J'(\mathbf{q})|| \ll \Delta_r$, is increasingly fulfilled by going from the lowest branch with r = I up to IV. We recognize that the intercluster couplings J_n listed in table 1 are comparable to the intracluster exchange parameters j, j' and j'' in magnitude. This was also concluded from a qualitative analysis of the Mn–Mn superexchange couplings based on the H–T phase diagrams of α-$MnMoO_4$ [14]. Nevertheless, the similar magnitudes of the intra and intercluster exchange parameters do not call the applicability of equation (6) into question, since the relevant energy scale is set by the energies Δ_r, for which the contribution of the parameters j, j' and j'' is enhanced by large prefactors; see equation (3). In other words, the predominantly ferromagnetic intracluster couplings give rise to quite robust tetramer states, whereas the net effect of the intercluster interaction is considerably damped due to the partial cancellation of the ferromagnetic and antiferromagnetic exchange parameters J_n.

The fact that the best fits A and C resulted in standard deviations of about $\chi^2 \approx 4$ points to some shortcomings of the dispersion model (equation (6)). A possible improvement of the model is to expand the excitation energies order by order in the inter-tetramer interactions. Such an approach was carried out for dimer spin systems [15]. It was found that, from the second order, new terms appear that are not present in the square root of equation (7). Another problem is related to the different nature of transitions I–IV, so that initial and final state effects have to be considered, i.e., the intercluster interactions J_{nm} have to be treated as tensors $J_{nm}(T_n^{\text{i}}, T_m^{\text{i}}; T_n^{\text{f}}, T_m^{\text{f}})$, where $T = \{S_{12}, S_{34}, S\}$, and the labels i and f refer to the initial and final states of the transition, respectively. The exchange tensor formalism was postulated as long as 40 years ago [16], but so far its relevance has only been demonstrated experimentally for the compounds $Cs_3Ho_2Br_9$ [17] and Nd_2CuO_4 [18]. For the lowest branch I the tensor formalism is irrelevant, since the transition is governed by $\Delta S_{12} = \Delta S_{34} = \Delta S = 0$ (see the inset of figure 2) and therefore resembles a classical spin-wave excitation. Accordingly, fit procedure B converged to an optimum standard deviation $\chi^2 = 1$, resulting in

partly different exchange parameters J_n as compared to fits A and C. Thus we may consider the parameters of fit B to be more reliable than those of fits A and C. This assumption is supported by a comparison of the observed and calculated molecular field, which is given by

$$H_{\mathrm{mf}} = \frac{2}{g\mu_{\mathrm{B}}} \sum_{\nu=1}^{4} \langle s_\nu^z \rangle \sum_{n=1}^{6} z_n J_n = \frac{2}{g\mu_{\mathrm{B}}} \langle S^z \rangle \sum_{n=1}^{6} z_n J_n, \quad (11)$$

where z_n is the number of nth nearest-neighbour tetramers. From neutron diffraction the saturation moment of the Mn^{2+} ions was determined to be $\langle s^z \rangle = 2.35$ and therefore $\langle S^z \rangle = 4\langle s^z \rangle = 9.4$ [10]. From the parameters of fit B we find $\sum z_n J_n = 44(32)$ μeV. Insertion into equation (11) yields $H_{\mathrm{mf}} = 7.1(4.9)$ T, which is comparable to $H_{\mathrm{mf}} = 5.4$ T determined from the energies Δ_r listed in table 1. On the other hand, the parameters of fit A yield $\sum z_n J_n = 188(85)$ μeV, resulting in an unrealistically large value of $H_{\mathrm{mf}} = 30(14)$ T.

The lowest acoustic branch I does not soften completely at the magnetic zone centres, but a gap of 0.28(4) meV remains. This is most likely a single-ion anisotropy. Assuming an axial anisotropy, this takes the form

$$\mathcal{H}_{\mathrm{an}} = D \sum_i (s_i^z)^2 \quad (12)$$

and yields the anisotropy parameter $D \approx 45(6)$ μeV. This is comparable to the gap energy of 0.4 meV reported for the related compound $MnWO_4$ [19].

In conclusion, the magnetic excitation spectra of the tetramer-based compound α-$MnMoO_4$, determined by single-crystal INS experiments, have been presented for wavevectors along different symmetry directions. The observed dispersion relations have been analysed with use of an RPA-like dispersion model which treats the intercluster interactions as a perturbation of the localized tetramer transitions. α-$MnMoO_4$ thus provides a model system to study the interplay of intra and intercluster interactions. In order to obtain quantitative results for the most important couplings between neighbouring tetramers, it was necessary to use a single crystal and to follow the various excitation branches by INS along all the relevant directions of the Brillouin zone. Such information is usually not available with molecular cluster materials, since these cannot be grown as 10 g single crystals.

Acknowledgments

This work was performed at the Swiss Spallation Neutron Source SINQ, Paul Scherrer Institut (PSI), Villigen, Switzerland. We thank N Cavadini, S Gvasaliya, Ch Niedermayer, and B Roessli for invaluable experimental support during the INS measurements. Financial support by the Swiss National Science Foundation is gratefully acknowledged.

References

[1] Gatteschi D and Sessoli R 2002 *Angew. Chem. Int. Edn* **42** 268 and references therein
[2] Sieber A, Foguet-Albiol D, Waldmann O, Ochsenbein S T, Bircher R, Christou G, Fernandez-Alonso F, Mutka H and Güdel H-U 2005 *Inorg. Chem.* **44** 6771
[3] Wernsdorfer W, Bhaduri S, Tiron R, Hendrickson D N and Christou G 2002 *Phys. Rev. Lett.* **89** 197201
[4] Mirebeau I, Hennion M, Casalta H, Andres H, Güdel H-U, Irodova A V and Caneschi A 1999 *Phys. Rev. Lett.* **83** 628
[5] Strässle Th, Juranyi F, Schneider M, Janssen S, Furrer A, Krämer K W and Güdel H-U 2004 *Phys. Rev. Lett.* **92** 257202
[6] Leuenberger B, Stebler A, Güdel H-U, Furrer A, Feile R and Kjems J K 1984 *Phys. Rev.* B **30** 6300
[7] Cavadini N, Heigold G, Henggeler W, Furrer A, Güdel H-U, Krämer K and Mutka H 2000 *J. Phys.: Condens. Matter* **12** 5463
[8] Ochsenbein S T, Chaboussant G, Sieber A, Güdel H-U, Janssen S, Furrer A and Attfield J P 2003 *Phys. Rev.* B **68** 092410
[9] Abrahams S C and Reddy J M 1965 *J. Chem. Phys.* **43** 2533
[10] Attfield J P 1990 *J. Phys.: Condens. Matter* **2** 6999
[11] Oguchi T 1955 *Prog. Theor. Phys.* **13** 148
[12] Oosawa A, Kato T, Tanaka H, Kakurai K, Müller M and Mikeska H-J 2002 *Phys. Rev.* B **65** 094426
[13] Jensen J and Mackintosh A R 1991 *Rare Earth Magnetism—Structures and Excitations* (Oxford: Clarendon)
[14] Ehrenberg H, Schwarz B and Weitzel H 2006 *J. Magn. Magn. Mater.* **305** 57
[15] Müller M and Mikeska H-J 2000 *J. Phys.: Condens. Matter* **12** 7633
[16] Levy P M 1969 *Phys. Rev.* **177** 509
[17] Furrer A, Güdel H-U, Krausz E R and Blank H 1990 *Phys. Rev. Lett.* **64** 68
[18] Henggeler W, Chattopadhyay T, Roessli B, Vorderwisch P, Thalmeier P, Zhigunov D I, Barilo S N and Furrer A 1997 *Phys. Rev.* B **55** 1269
[19] Ehrenberg H, Weitzel H, Fuess H and Hennion B 1999 *J. Phys.: Condens. Matter* **11** 2649